RSC Advances

PAPER

View Article Online
View Journal | View Issue

Cite this: *RSC Adv.*, 2026, **16**, 5325

Catalytic wet air oxidation of phenol in caustic refinery effluents

Jorge F. Palomeque-Santiago *[a] and José J. Castro-Arellano [b]

Phenol, in industrial aqueous effluents, causes serious damage to human health and ecosystems due to its high toxicity. Catalytic wet air oxidation (CWAO) is a process that effectively transforms phenol into compounds with lower environmental impact. The development of catalysts capable of operating continuously without activity loss in industrial effluents is a challenge due to metal leaching deactivation caused by the formation of organic acids during oxidation reactions. In particular, effluents from caustic treatments in refineries extract large amounts of phenol and their treatment by CWAO has not been widely addressed. In the present study, CuO and ZnO catalysts were synthesized by employing different aluminum-based supports, which not only achieved high phenol oxidation in neutral aqueous solutions, but also increased the phenol degradation degree with great stability in a refinery sample from caustic treatment, making CWAO viable for processing industrial effluents.

Received 30th October 2025
Accepted 26th December 2025

DOI: 10.1039/d5ra08364h

rsc.li/rsc-advances

1 Introduction

Refineries and petrochemical plants are currently making efforts to resolve their problems of disposing of polluting streams. Water pollution has reached levels that affect all types of aquatic life, causing serious problems for human health. Pollution generated at industrial centers is one of the most difficult to deal with because the discarded compounds are not easily eliminated by natural biological degradation or treatment processes.[1,2] Light and intermediate oil cuts contain high concentrations of sulfur such as hydrogen sulfide, mercaptans, and thiophenes, which are removed with different treatments according to their reactivity. Thiophenes are cyclic compounds that are difficult to remove and require high pressure and temperature through the hydrodesulfurization process. H_2S and mercaptans are low molecular weight compounds and are removed by means of caustic processes, in which the hydrocarbon and a caustic solution are brought into close contact, transforming them into sodium sulfide and disulfides, thereby minimizing their adverse corrosive characteristics and unpleasant odors. Additionally, caustic soda extracts phenols, cresols, mercaptans, organic and inorganic acids, fats, and oils, which, once integrated into the alkaline aqueous medium, become pollutants that are difficult to dispose of.[3,4]

Since phenol is considered as a high risk to human, animal and plant life forms, its discharge into receiving bodies such as rivers or lagoons is very restricted. Spent soda produced in refining plants has different characteristics depending on the type of crude oil, sweetening process, and treated hydrocarbon fraction. The caustic streams used in the treatment of hydrocarbons contain considerable amounts of phenol, up to 8–12 wt%, which due to their toxicity, represent a serious problem.

Catalytic wet air oxidation (CWAO) is a good alternative for the treatment of caustic solutions generated in refineries. Organic compounds are oxidized to carbon dioxide and water in the presence of a catalyst under mild conditions (403–423 K and 0.5–1.5 MPa); however, its application to real industrial effluents remains limited by catalyst deactivation caused by metal leaching during oxidation. In particular, the treatment of caustic refinery effluents by CWAO has not been previously addressed, despite their high phenol content.

Oxygen is the most commonly used oxidant in CWAO, but H_2O_2 has also been reported to obtain faster oxidation and mineralization rates due to the reaction initiation by hydroperoxy radicals.[5,6] Notwithstanding, this oxidant is more expensive than oxygen taken from air and the process becomes more expensive.

The CWAO process has been studied in the homogeneous phase using Fe and Cu salt catalysts with oxygen as the oxidant. The heterogeneous phase process with solid catalysts is more practical since the catalyst separation step is avoided. Many factors such as temperature, pressure, oxygen partial pressure, pH, types of organic compounds to be oxidized, as well as reactor design influence this process. Various intermediate products are formed during the oxidation process, including catechol, hydroquinone, benzoquinones, and organic acids, the latter being among the last compounds generated before CO_2. Dissolved oxygen plays an important role since the reaction

[a]*Instituto Mexicano del Petróleo, Av. Eje Central Lázaro Cárdenas Norte 152, Col. San Bartolo Atepehuacan, C. P. 07730, Ciudad de México, Mexico. E-mail: jpalomeq@imp.mx*

[b]*Escuela Superior de Ingeniería Química e Industrias Extractivas - Instituto Politécnico Nacional, Edificio 8, 3er piso, Col. Zacatenco, Gustavo A. Madero, C. P. 07738, Ciudad de México, Mexico*

mechanism includes the formation of free radicals and bimolecular reactions between the organic compounds and oxygen.[7,8]

Some of the catalysts used in the phenol oxidation process are metals such as platinum, palladium, ruthenium, and rhodium. The advantages of noble metals are their high activity, obtaining elevated conversions at low pressure and temperature in short times. The incorporation of metals such as Mn and Ce improves the performance of the catalysts, obtaining higher mineralization rates and less deposition of carbonaceous compounds on the catalyst surface, however, their high cost is an impediment to their large-scale implementation.[9,10] Mixtures of non-noble metal oxides such as Mn, Ce, Fe, Si, Cu, Zn, Co, and Ni, among others, have also been investigated; the catalytic activity of these catalysts is greatly influenced by the catalyst composition, textural properties, particle size, structural characteristics, and oxidation state. Good activities were obtained with metals with higher oxidation states such as Mn^{4+}, and Fe^{3+}, due to their high reducibility.[11–13] The incorporation of Ce helps retaining the structure of the catalyst and prevents Mn^{4+} or Mn^{3+} from being reduced to Mn^{2+}.[14] Active carbon has good properties as adsorbent of phenol and oxygen achieving high phenol conversions but with rapid deactivation due to leaching and surface area reduction.[15,16]

Copper oxides have been studied since 1974 by Sadana and Kaltzer, proving to be efficient catalysts for the oxidation of phenol in water.[8,17] Levec studied the oxidation of phenol in aqueous solutions using a catalyst consisting of copper oxide, zinc oxide and alumina in a three-phase reactor at total pressure of 0.6 MPa and 403 K, obtaining total phenol removal in 100 min.[18,19] In these systems, calcination temperature plays an important role because of the formation of aluminates; on the other hand, lixiviation of metals is mainly due to the formation of acid intermediates, that cause a drop in pH, involving a heterogeneous-homogeneous free radical mechanism. The improvement of catalysts to minimize leaching, increase metal dispersion and decrease metal loading has been the subject of much work, in which Cu and Zn have shown good results for phenol oxidation, where some commercial catalysts have been taken as reference for some studies.[16,20–23]

Many attempts have been made to minimize lixiviation, and to this end, alumina-supported metals have been found to generate less leached metals than bulk catalysts, obtaining higher phenol conversions, being homogeneous reactions responsible for limiting activity.[20,22,24] The incorporation of Mn into alumina-supported copper anchors Cu to the support with less leaching.[25] Spinels are formed during heat treatment at elevated temperatures by the interaction of a divalent metal cation and a trivalent metal cation, forming a close-packed cubic crystal centered on the oxygen faces, where the octahedral and tetrahedral holes are partially occupied. These structures are very stable and excellent catalytic supports and have been successfully used in the oxidation of phenol.[26–28] Spinels show lower leaching of active metals with high phenol conversions.[29–31] The structure of the spinel $Cu_{0.5-x}Fe_xZn_{0.5}Al_2O_4$, has proved to be highly resistant to dissolution in acidic fluids, reducing the amount of leached copper.[32]

The CWAO process has been widely used in the degradation of organic compounds in aqueous streams from the pharmaceutical industry, municipal waters, and petroleum industry waste streams with high hydrocarbon contents. In this context, leaching can be minimized at high pH, and Santos *et al.* achieved low copper leaching at pH 8 and constant phenol oxidation with time.[33,34] Other studies at higher pH have also been reported with low metal leaching.[35,36] Despite the extensive research on CWAO for phenol degradation in synthetic or neutral aqueous solutions, the application of this process to real caustic refinery effluents has not been reported, mainly due to concerns related to catalyst deactivation and metal leaching under severe reaction conditions. Moreover, the role of catalyst structure and metal–support interactions in controlling both activity and stability in alkaline industrial streams remains poorly understood.

Other processes reported for the treatment of refinery streams are Fenton oxidation, electrochemical oxidations, and biological treatment, among others.[37–41] However, these streams must be previously neutralized; furthermore, biological treatment cannot work with high concentrations of phenol, since its toxicity impacts the microorganisms responsible for its decomposition.[42–44]

In this work, CuO- and ZnO-based catalysts were synthesized using different aluminum-based supports, including bulk oxides, γ-Al_2O_3-supported materials, and aluminate spinels. The catalysts were evaluated for phenol oxidation under CWAO conditions in both neutral aqueous solutions and real caustic refinery effluents. The results show that alumina- and aluminate-supported catalysts significantly enhance phenol degradation while suppressing metal leaching, even in the presence of oxidation-derived organic acids. CuO supported on zinc aluminate exhibited high phenol conversion and remarkable stability during multiple runs in alkaline refinery samples, where organic acids were neutralized by NaOH.

These findings demonstrate that properly designed Cu–Al and Zn–Al catalysts enable stable and efficient CWAO operation with real caustic refinery effluents, providing a viable route for the treatment of spent caustic streams in industrial applications. The catalytic materials were characterized and evaluated to identify the most promising materials for industrial use in the treatment of caustic refinery effluents.

2 Materials and methods

2.1 Catalysts preparation

Three types of catalysts were prepared from aqueous solutions of the metal salts in quantities calculated according to Table 1. Bulk catalysts (B) were prepared by coprecipitation of the metal salts with 30% aqueous NH_4OH solution at 343 K and pH = 7, controlled with 1N HNO_3. Powders were filtered, washed with distilled water and dried in an oven at 393 K during 12 h. The thermal treatment was performed under air environment at 873 K for 4 h with a heating ramp of 10 K min^{-1}. Catalysts impregnated with CuO and ZnO (MO/Al_2O_3, where M = Cu or Zn) were synthesized by incipient wetting with γ-alumina CS 331–1 (Süd-Chemie A. G., Germany) with BET surface area of

Table 1 Target concentration of catalysts

Catalyst name	Composition, wt%				
	CuO	ZnO	Al_2O_3	$CuAl_2O_4$	$ZnAl_2O_4$
B-1	40	60	0	0	0
B-2	10	90	0	0	0
B-3	30	50	20	0	0
B-4	30	60	10	0	0
Cu-1/Al_2O_3	3	0	Balance	0	0
Cu-2/Al_2O_3	5	0	Balance	0	0
Cu-3/Al_2O_3	10	0	Balance	0	0
Cu-4/Al_2O_3	15	0	Balance	0	0
Zn-1/Al_2O_3	0	3	Balance	0	0
Zn-2/Al_2O_3	0	5	Balance	0	0
Zn-3/Al_2O_3	0	10	Balance	0	0
Zn-4/Al_2O_3	0	15	Balance	0	0
Zn-1/$CuAl_2O_4$	0	3	0	Balance	0
Zn-2/$CuAl_2O_4$	0	5	0	Balance	0
Zn-3/$CuAl_2O_4$	0	10	0	Balance	0
Zn-4/$CuAl_2O_4$	0	15	0	Balance	0
Zn-5/$CuAl_2O_4$	0	20	0	Balance	0
Zn-6/$CuAl_2O_4$	0	25	0	Balance	0
Cu-1/$ZnAl_2O_4$	3	0	0	0	Balance
Cu-2/$ZnAl_2O_4$	5	0	0	0	Balance
Cu-3/$ZnAl_2O_4$	10	0	0	0	Balance
Cu-4/$ZnAl_2O_4$	15	0	0	0	Balance
Cu-5/$ZnAl_2O_4$	20	0	0	0	Balance
Cu-6/$ZnAl_2O_4$	25	0	0	0	Balance
Cu-7/$ZnAl_2O_4$	30	0	0	0	Balance

255 $m^2 g^{-1}$ and pore volume of 0.76 $cm^3 g^{-1}$. After drying during 12 h in an oven at 293 K, the materials were calcined at 873 K for 6 h with a heating ramp of 10 K min^{-1}. Copper and zinc oxides over spinels ($M_1O/M_2Al_2O_4$, where M_1 and M_2 = alternating Cu or Zn) were obtained in two steps: copper and zinc aluminate supports were prepared separately by coprecipitation from stoichiometric amounts of nitrate salts with 30% aqueous NH_4OH solution at 343 K and pH = 7.5, controlled with 1N HNO_3. The solids were filtered, washed with hot deionized water and dried during 12 h in an oven at 393 K. The thermal treatment was performed under air atmosphere at 1173 K for 12 h. Different amounts of CuO and ZnO were impregnated by incipient wetting over the spinels, dried at 393 K with a final treatment under air environment at 873 K for 4 h with a heating ramp of 10 K min^{-1}. The target compositions are shown in Table 1.

2.2 Characterization of catalysts

Metal content was determined by plasma emission spectrophotometry in a PerkinElmer 5000 spectrometer. Textural analyses were obtained under vacuum by nitrogen physisorption in an ASAP- 2405 analyzer from Micromeritics. Powder X-ray diffraction patterns were obtained in a D-500 siemens diffractometer with CuKα1 radiation. Scanning electron microscopy analysis was performed by using a JEOL 440 scanning electron microscope operated at accelerating voltage of 25 kV and 20.000× magnification. Transmission electron microscopy (TEM) analyses of the samples were carried out in a JEOL 2010F microscope operating at 200 kV.

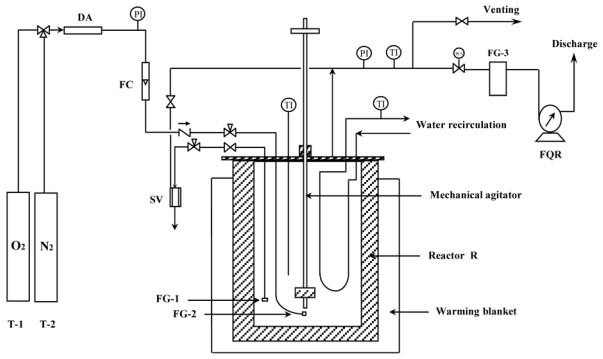

Fig. 1 Catalytic evaluation system.

2.3 Catalytic evaluation

The catalytic evaluation of the catalysts was carried out in a 1-liter stainless steel semi-batch reactor. The diagram of the experimental system is shown in Fig. 1. The system consists of the components listed in Table 2.

The catalysts were introduced into the reactor in powder form. Reactor R operated with continuous flow of oxygen supplied by T-1 to perform oxidation. However, during the plant stabilization period, the gas flow was supplied with nitrogen *via* T-2 to prevent premature reactions. An FG-2 bubbler was placed at the gas inlet to the reactor to feed oxygen in fine bubbles. Once the reaction conditions were reached, nitrogen was replaced by oxygen using a three-way valve, with the reaction time being set to zero. The gas flow was controlled by an FC mass flow controller. To prevent phenol leaks into the atmosphere, an FG-3 scrubber filter containing 1 N sodium hydroxide solution was placed in the outlet line. Sampling was carried out with a needle valve, and a sintered metal filter was placed at the inlet of the FG-1 sampling line to prevent catalyst carryover.

Phenol disappearance was monitored by an HP 580 gas chromatograph with flame ionization detector equipped with a 5% diphenyl-95% dimethyl silicone crosslinked copolymer capillary column, 25 m long × 0.22 mm internal diameter and 0.33 μm film thickness. The calibration curve was performed with phenol (99.97%, Baker) and methanol (99.9%, Baker) solutions at known concentrations. The reaction intermediate compounds were determined by means of a Hewlett Packard 5890 Series II gas chromatograph/mass spectrometer/5971 with a 5% PhMe silicone column (0.5 mm i.d., 30 m long, 2.65 μm

Table 2 Components of the catalytic evaluation system

Reactor, R	Pressure gauges, PI
Oxygen tank, T-1	Temperature gauges, TI
Nitrogen tank, T-2	Sampling valve, SV
Desiccant column, DA	Needle valves
Fine filter, FG-1	Gate valves
Gas dispersion filter (bubbler) FG-2	Three-way valve
Gas filter, FG-3	Pressure control valve
Mass flow controller, FC	Check valve
Gasometer, FQR	—

Table 3 Catalytic evaluation conditions

Condition	Value
Temperature, K	403
Total pressure, MPa	0.6
Phenol concentration, wt%	1
Reaction time, h	6
O_2 flow rate, mL min^{-1}	250
Catalyst mass, g	3
Reaction volume, mL	500
Stirring speed, rpm	500

thickness) and a phase ratio of 50. Data were collected in the 373–423 K temperature interval. The molecular ionization energy was 70 eV with emission current of 200 μA. The lowest limit of mass detection after calibration was mass = 1.

The evaluation conditions of all the catalysts were set as shown in Table 3.

3 Results

3.1 Composition and textural analysis

The results of atomic absorption and textural analysis of the catalysts are shown in Table 4.

Bulk catalysts had low surface area, which increased by twofold with the addition of small amounts of alumina (B-3 and B-4); the pore volume and pore diameter also increased in the same proportion. The alumina-supported catalysts had the highest surface areas, which decreased as a greater amount of copper or zinc was impregnated; a decrease of 8.82% for copper catalysts and 4.82% for zinc catalysts were observed. The same phenomenon occurred with pore volume values; however, pore diameters remained within the same interval of values. The aluminate catalysts had much smaller surface areas, notwithstanding, the obtained pore diameters were larger. As for the copper aluminate-supported catalysts, they displayed even lower surface areas than zinc-aluminate catalysts and pore volumes were 10 times smaller than in zinc aluminate. Pore diameters remained within the same range. It is also worth noting that the Zn content in copper aluminates no longer increased compared to what was planned with higher concentration solutions, perhaps reaching saturation due to the very low pore volumes and surface areas.

3.2 X-ray diffraction

Fig. 2 shows the X-ray diffraction patterns of the catalysts prepared using the different synthesis routes. Rietveld refinement (RR) was performed using HighScore Plus v. 4.9. For

Table 4 Composition and textural analysis of the catalysts

	Composition, wt%			Textural analysis		
Catalyst name	Cu	Zn	Al	Surface area $m^2\ g^{-1}$	Pore volume $cm^3\ g^{-1}$	Pore diameter Å
Bulk						
B-1	32.9	45.6	0	25.7	0.104	64
B-2	6.3	73.8	0	26.8	0.162	94
B-3	22.1	43.1	5.7	58.8	0.235	134
B-4	23.2	47.8	4.2	39.8	0.183	103
Supported on γ-alumina						
Cu-1/Al_2O_3	5.2	0	41.7	238	0.681	115
Cu-2/Al_2O_3	7.8	0	42.8	234	0.754	128
Cu-3/Al_2O_3	10.9	0	41.2	221	0.652	117
Cu-4/Al_2O_3	14.3	0	39.5	217	0.623	114
Zn-1/Al_2O_3	0	3.7	42.8	228	0.714	124
Zn-2/Al_2O_3	0	5.1	41.8	225	0.687	122
Zn-3/Al_2O_3	0	7.3	41.9	218	0.672	123
Zn-4/Al_2O_3	0	7.8	40.7	217	0.671	125
Supported on copper aluminate						
Zn-1/$CuAl_2O_4$	21.5	1.8	25.4	14	0.052	157
Zn-2/$CuAl_2O_4$	20.7	2.8	24.6	12	0.053	172
Zn-3/$CuAl_2O_4$	21.7	9.2	26.2	12	0.046	159
Zn-4/$CuAl_2O_4$	21.3	9.0	25.1	11	0.046	165
Zn-5/$CuAl_2O_4$	21.2	9.2	24.8	11	0.048	181
Zn-6/$CuAl_2O_4$	20.9	9.3	24.9	12	0.047	175
Supported on zinc aluminate						
Cu-1/$ZnAl_2O_4$	2.2	29.5	24.4	32	0.159	200
Cu-2/$ZnAl_2O_4$	3.6	29.7	24.6	31	0.149	191
Cu-3/$ZnAl_2O_4$	7.1	28.8	24.2	30	0.141	190
Cu-4/$ZnAl_2O_4$	8.4	30.3	25.1	29	0.134	187
Cu-5/$ZnAl_2O_4$	11.8	31.0	25.8	28	0.117	169
Cu-6/$ZnAl_2O_4$	12.9	29.2	24.3	26	0.138	215
Cu-7/$ZnAl_2O_4$	16.5	29.9	24.9	25	0.116	184

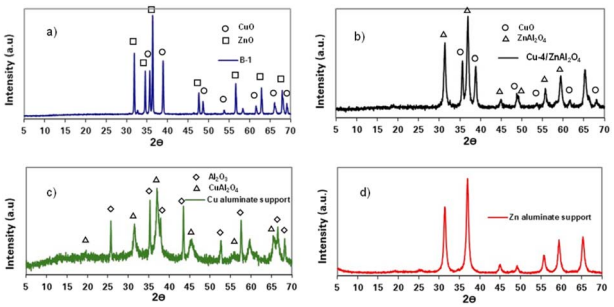

Fig. 2 X-ray diffraction patterns of (a) bulk, (b) Cu/Zn aluminate, (c) Cu aluminate support, and (d) Zn aluminate support.

Table 5 Particle size distribution of the catalysts

Particle size μm	Bulk-3	Cu-4/Al_2O_3	Cu-7/$ZnAl_2O_4$	Zn-6/$CuAl_2O_4$
20	75.3	92.8	67.3	33.2
40	21.9	5.2	27.1	41.5
60	0.9	0.4	1.5	20.3
80	0.5	0	0.7	5.0
100	0.9	0.8	0.0	0.0
120	0.5	0.4	0.0	0.0
140	0.0	0.4	0.4	0.0
160	0.0	0.0	1.1	0.0
>160	0.0	0.0	1.9	0.0
Total	100	100.0	100.0	100.0

clarity, only one representative diffractogram is shown for each catalyst series, since the main structural differences among samples within the same series arise from variations in metal loading rather than phase composition.

The diffraction pattern of the bulk catalyst (B-1), shown in Fig. 2a, reveals the coexistence of CuO (tenorite, JCPDS 41-0254) and ZnO (zincite, JCPDS 36-1451) as the only crystalline phases. Rietveld analysis indicates a phase composition of 63.6 wt% ZnO and 36.4 wt% CuO, confirming the formation of a mixed CuO–ZnO oxide system without secondary alumina-containing phases.

The diffractogram corresponding to the zinc aluminate support, presented in Fig. 2d, shows exclusively the characteristic reflections of the $ZnAl_2O_4$ spinel phase (JCPDS 05-0669). The absence of additional crystalline phases and the Rietveld result ($ZnAl_2O_4$ = 100 wt%) confirm the successful synthesis of a single-phase zinc aluminate support.

In contrast, Fig. 2c displays the diffraction pattern of the copper aluminate support, where reflections associated with the $CuAl_2O_4$ spinel (JCPDS 33-0448) are observed together with residual Al_2O_3 (corundum). Rietveld refinement yields a composition of 63 wt% $CuAl_2O_4$ and 37 wt% Al_2O_3, indicating that during the support synthesis the hydroxide precursors were not fully stoichiometrically precipitated, leaving an excess of alumina in the final material.

Finally, Fig. 2b corresponds to the catalyst prepared by depositing copper oxide on the zinc aluminate support. The diffraction pattern confirms the preservation of the $ZnAl_2O_4$ spinel structure, together with additional reflections assigned to CuO. Rietveld analysis reveals a phase composition of 87.6 wt% $ZnAl_2O_4$ and 12.4 wt% CuO, evidencing the successful deposition of CuO on the aluminate support without significant disruption of the spinel framework.

Overall, the results confirm that the different preparation methods led to well-defined crystalline phases, and that the nature of the support (bulk oxide, alumina, or aluminate spinel) strongly influences the final phase composition and structural integrity of the catalysts.

3.3 Electron microscopy

Scanning electron microscopy was used to determine the metal distribution in the catalysts; micrographs showed that in all cases there was a uniform distribution of both copper and zinc, so that both coprecipitation and impregnation preparations were carried out successfully and without concentration gradients. Fig. 3 presents the micrographs of the Cu-7/$ZnAl_2O_4$-catalyst, which was the most evaluated. The metallic particle size distribution was determined by scanning transmission electron microscopy; the results of a representative catalyst for each prepared series are presented in Table 5.

The largest particle size distribution was concentrated mainly in the 20 μm range for all the catalysts. The alumina-impregnated catalyst showed a 93% particle size distribution in the 20 μm range, with a very low proportion of larger sizes. The particle size distribution in the aluminate-supported catalysts concentrated along the size interval ranging from 20 to 60 μm.

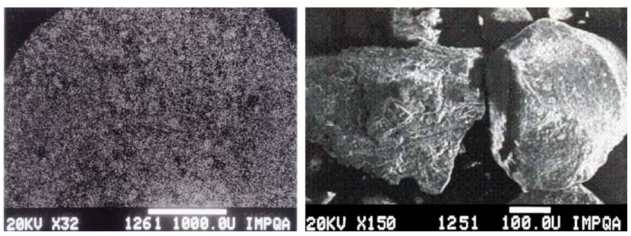

Fig. 3 Micrographs of the Cu-7/$ZnAl_2O_4$ catalyst.

4 Catalytic evaluation

4.1 Phenol oxidation

All the catalysts were tested in an aqueous phenol-water solution at 0.6 MPa and 403 K to compare their catalytic activity in the phenol oxidation reaction. The reaction time was 6 h, and samples were taken every hour for chromatographic analysis. Fig. 4 shows the phenol conversion obtained for the bulk catalysts. Only the phenol conversion as a function of time is shown for the catalyst with the highest conversion.

The Bulk-3 catalyst was the one that presented the highest phenol conversion, and this may be due to the larger pore diameter. The assumption was reinforced by the behavior pattern displayed by the Bulk-2 catalyst, which although presented lower Cu concentration (6.3%), the pore diameter of 94

was a determining factor in the phenol conversion, and being a mass catalyst, this concentration had a lesser effect than the pore diameter. It is also believed that zinc imparted certain synergy to copper, and that even at low Cu concentrations of the Bulk-2 catalyst, Zn helped keep its activity.

The growth mechanism of the metal active sites can be described as follows:

$$M^{2+}\,(aq) \rightarrow \text{homogeneous nucleation} \rightarrow M(OH)_2 \rightarrow MO + H_2O \rightarrow \text{oxide crystallites}$$

Bulk CuO–ZnO catalysts exhibited activity trends that correlated with their textural properties. In particular, the presence of γ-Al_2O_3 in B-3 and B-4 enhanced dispersion, with B-3 (93% conversion) being the most active and B-4 (81%) showing intermediate yet robust performance (Table 4 and Fig. 4).

The studies conducted on the oxidation of phenol with alumina-impregnated catalysts indicated the formation of spinels during calcination, being responsible for the increase in the phenol oxidation degree.[18,22] The induction period reported by different authors was not appreciated in the present work since the first sample was taken at 60 min. Fig. 5 shows the evaluation results of the catalysts supported on alumina with copper and zinc oxides, severally.

A clear relationship between the metal loading and phenol conversion was appreciated as reported by other authors.[20,24,45] The Cu concentration in the alumina catalysts showed a conversion increase of 25% with a 9.1% increase in Cu concentration (see Table 4), notwithstanding, the zinc oxide catalysts had greater influence since with a small increase in the metallic concentration of 4.7%, the conversion increased in a greater proportion by 47%. This may have been caused by the critical catalyst concentration (CCC), a phenomenon reported by different authors, where with a small increase in catalyst concentration, the kinetic reaction rate increases dramatically. A higher catalyst concentration tended to improve the reaction rate because there were more active sites where the reactants could react, and consequently the reaction processes were accelerated. Sadana found through kinetic studies that this critical concentration was related to the concentration of hydroperoxides in the solution and to the oxygen partial pressure, but also to the substrate type, catalyst surface area and temperature.[46,47]

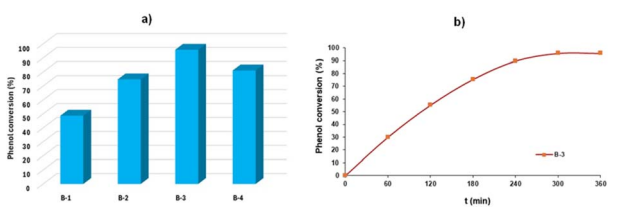

Fig. 4 Phenol conversion with the bulk catalysts: (a) B1–B4, (b) phenol conversion as a function of time for B-3. (Reaction conditions: temperature = 403 K, pressure = 0.6 MPa, [phenol] = 1 wt%).

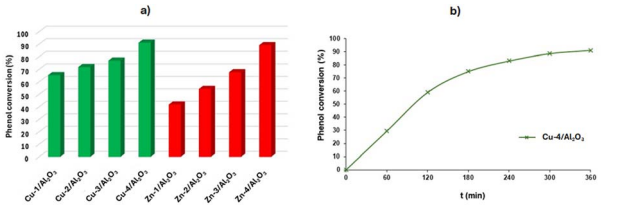

Fig. 5 Phenol conversion with the alumina-supported catalysts: (a) Cu/Al_2O_3 and Zn/Al_2O_3, (b) phenol conversion as a function of time for Cu-4/Al_2O_3. (Reaction conditions: temperature = 403 K, pressure = 0.6 MPa, [phenol] = 1 wt%).

In this case, there was strong chemisorption of CuO and ZnO on surface hydroxyl groups and γ-Al_2O_3-supported catalysts displayed progressively enhanced conversion with increasing metal loading, with Cu showing higher degradation rates than Zn. This behavior reflected the stabilizing role played by surface hydroxyls in maintaining highly dispersed oxide nanodomains, consistent with the larger BET surface areas observed for these samples.

$$(\equiv Al\text{–}OH) \text{ of } \gamma\text{-}Al_2O_3 \rightarrow \text{anchored } M(OH)_2 \text{ species} \rightarrow \text{formation of highly dispersed 2D CuO/ZnO domains.}$$

The catalytic evaluation of the aluminate-supported catalysts was carried out under the same conditions. The results for these catalysts are shown in Fig. 6.

Phenol oxidation by the zinc oxide on Cu aluminate became constant, since the Zn concentration also remained at similar values close to 9% (Table 4); the same phenomenon occurred in the alumina-supported catalysts, however, unlike these catalysts, increasing the metallic loading of Zn did not significantly increase conversion. Low surface areas and pore volumes could have had a significant effect on this behavior.

Comparatively, these catalysts delivered lower activity (27–54%), which was attributable to restricted dispersion of ZnO on the compact spinel surface. Only the first three samples exhibited an increase in phenol conversion with Zn loading, which was likely due to deviations between nominal and actual Zn incorporation (Table 4, Fig. 6a, blue).

The growth mechanism of ZnO on Cu spinel can be described as:

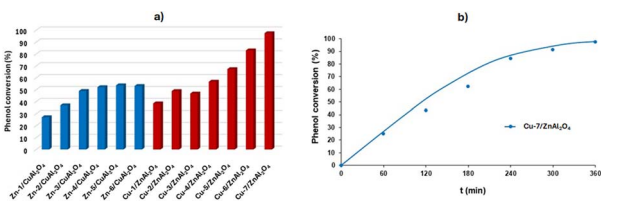

Fig. 6 Phenol conversion with the aluminate-supported catalysts: (a) $Zn/CuAl_2O_4$ and $Cu/ZnAl_2O_4$, (b) phenol conversion as a function of time for Cu-7/$ZnAl_2O_4$. (Reaction conditions: temperature = 403 K, pressure = 0.6 MPa, [phenol] = 1 wt%).

Low density of hydroxyl groups → $Zn(OH)_2$ formation at defect sites → poorly dispersed ZnO clusters.

In contrast with the Zn-loaded spinels, $Cu/ZnAl_2O_4$ catalysts showed a marked increase in conversion with growing Cu content (Fig. 6a, red). These materials achieved surface areas nearly twice those of $Zn/CuAl_2O_4$ and reached up to 97.5% conversion for $Cu\text{-}7/ZnAl_2O_4$, which was in agreement with the formation and robust anchoring of CuO nanoparticles on the spinel surface. A direct correlation with the copper metal concentration could be appreciated, where the presence of Zn could modify the dispersion of CuO and favor the formation of active sites leading to higher Cu concentrations than in alumina. The low metal loading in these catalysts sets them as promising materials to be applied in this process.

Cu^{2+} anchoring on surface oxygen → Cu $(OH)_2$ → CuO nanoparticle nucleation → activity scaling with Cu loading.

This mechanistic framework aligns fully with the catalytic results, demonstrating that the interplay between oxide dispersion, anchoring strength, and support surface chemistry governs the degradation efficiency.

Overall, these trends confirm that catalytic activity is dictated by the structure and surface chemistry of the support, which determines the growth mode, dispersion, and accessibility of the active species.

4.2 Analysis of the reaction effluent

The reaction effluents were analyzed using mass spectrometry to identify reaction intermediates. This study indicated that various byproducts were formed during the oxidation of phenol through consecutive reactions. The found byproducts were catechol, hydroquinone, *p*-benzoquinone, *o*-benzoquinone, di(4-hydroxyphenyl)ether, and di(2-hydroxyphenyl)ether; on the other hand, acetic and oxalic acids were the main identified acids. Several authors have reported on the formation of similar compounds and concluded that oxidation reactions were carried out by contributions from both the heterogeneous and homogeneous parts, where polymerization reactions occurred only in homogeneous-type reactions following a free-radical reaction route. On the other hand, oxalic acid, maleic acid, and benzoquinone were formed in both homogeneous and heterogeneous phases; heterogeneous reactions follow the surface-controlled Langmuir–Hinshelwood kinetic model. This means that CuO and ZnO leached and once in the aqueous medium, acted as catalysts contributing to reactions taking place in both heterogeneous and homogeneous phases.[26,48–50] According to these results, the reaction scheme in Scheme 1 is proposed for the oxidation of phenol in aqueous medium when oxygen is used as oxidizing agent.

This reaction pathway aligns well with earlier findings.[48,51,52] The oxidation of phenol occurs through a Cu^{2+}-catalyzed free-radical mechanism, whereby phenoxy radicals are formed *via* hydrogen abstraction from the aromatic ring, accompanied by the reduction of Cu^{2+} to Cu^{+}. Catechol and hydroquinone are

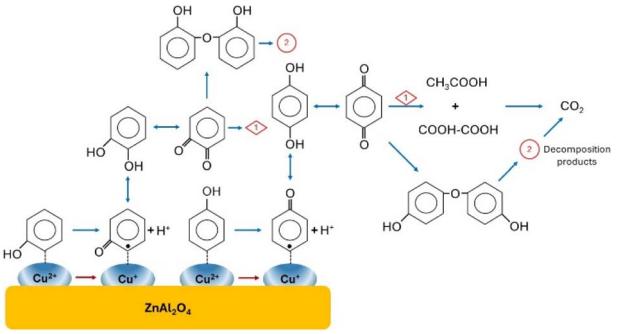

Scheme 1 Proposed reaction scheme for the oxidation of phenol with oxygen.

the first intermediates, which were further oxidized to *o*-benzoquinone and *p*-benzoquinone, severally. The ring opening of the aromatic compounds leads to the formation of short chain acids and CO_2. Oxalic and acetic acids are produced *via* other acid intermediates, such as formic, maleic, malonic, and fumaric acids.

The formation of dimers and polymeric products occur under special conditions; these compounds were not formed in a trickle-bed triphasic tubular reactor because of the high solid-to-liquid phase ratio,[49] and some metals such as platinum inhibit the polymerization reactions.[9] Polymers are produced by molecular coupling of aldehydes catalyzed in homogeneous phase. In a batch reactor, there is better catalyst wetting leading to lixiviation of metals, and oligomers are obtained at low catalyst loading, being further oxidized to acid intermediates.[48,52,53]

The pH of the reaction effluent was monitored to determine whether the formed byproducts influenced the variation in acidity. The effluent was also characterized to determine whether metal leaching occurred during the reaction. This monitoring was performed over time using atomic absorption analysis in the rection with the B-3 catalyst, and the obtained results are presented in Table 6.

From Table 6, it can be observed that pH decreased and the metal content in the effluent rose as the reaction progressed. This fact indicates that metallic leaching of the oxides contained in the catalyst did occur, with Zn being the metal most strongly influenced by pH. Other organic acids responsible of the pH drop have been oxalic acid, acetic acid, succinic acid, malonic acid, maleic acid and fumaric acid.[26,48,54,55] This metallic leaching causes the solid catalyst to gradually deactivate due to the loss of metallic content, and the leached metallic species, once integrated into the aqueous medium, act as homogeneous-phase catalysts, also promoting oxidation reactions.

4.3 Influence of temperature and pressure

Some tests were performed to determine the temperature influence on the phenol oxidation reaction taking place at 403, 423 and 448 K. All other operating conditions were kept constant. The best catalyst, $Cu\text{-}7/ZnAl_2O_4$, attained 100% of

Table 6 pH variation and metal characterization in the reaction effluent

Reaction time h	pH	Al ppm	Cu ppm	Zn ppm
1	6.3	<5	13	10
3	5.8	<5	14	77
4	5.3	<5	17	96
5	5.0	<5	20	124
6	4.3	<5	25	150

phenol conversion at 423 K. In order to see the real influence of temperature on the reaction, the catalyst B-1 was selected, and the results are shown in Fig. 7. At 423 K, the phenol conversion increased considerably; beyond this temperature, it is no longer advisable to work since it would increase the cost of the process. Temperature decreases the solubility of oxygen in water but increases the generation of free radicals. Furthermore, higher temperatures increase reaction rates according to Arhenius's Law. Increasing temperature affects the distribution of reaction products, since organic acids are more refractory to oxidation; some studies have found that with increasing temperature, there is greater formation of these compounds, as well as greater mineralization.[56,57]

A study of the influence of pressure on the oxidation of phenol was carried out, using B-1 as catalyst (Fig. 8). The temperature was maintained at 403 K. The reaction was favored at 1.5 MPa and ceased to have influence on higher pressures values. Increasing pressure also increases the generation of free radicals and intermediate active species and additionally increases the solubility of oxygen in water according to Henry's law. The fact that pressure no longer influences phenol removal from 2 MPa may be related to over-oxidation of the active metal species due to a more oxidative environment.[56] Another possible explanation is given by Rivas *et al.* who suggested that at higher oxygen concentrations, the production of intermediate species may affect oxygen solubility and the process kinetics.[58]

4.4 Catalyst stability

Experiments were performed with the Cu-7/$ZnAl_2O_4$ and B-3 catalysts through reuse experiments to determine catalyst deactivation. Reaction conditions were maintained according to Table 3; the catalysts were washed with hot water and dried at 393 K after each reaction cycle as recommended by some authors.[59,60] The activity of the Cu-7/$ZnAl_2O_4$ catalysts was maintained after 7 cycles showing good stability in the conversion of phenol with an average conversion of 90.4%. Phenol conversion with catalyst B-3 displayed peaks and valleys in phenol conversion, probably due to the efficiency of removing intermediate reaction species deposited on the surface of the catalyst that were eliminated at the washing stage. After the sixth run, the conversion decreased (Fig. 9).

These deposits caused fouling and deactivation of the catalyst and once these species were deposited on the catalyst, their desorption was very slow. These deposits can be removed by increasing the reaction temperature and this procedure can be a way to increase catalyst activity in continuous operation. Another way to remove them from the catalyst is through washing with hot water and organic solvents or by direct calcination at high temperature.

It has been well established in the literature that the species deposited on the catalyst are condensation and polymerization products, from which dimers, oligomers, biphenyls, and diphenyl ethers have been identified. These compounds are responsible for the dark brown color of effluents subjected to CWAO.[61] Hamoudi *et al.* reported that a platinum catalyst promoted with Mn and Ce or Ag presented low deposits of organic compounds and high phenol mineralization.[9]

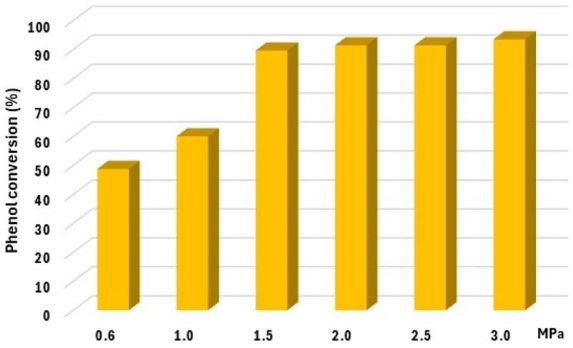

Fig. 8 Influence of pressure on phenol oxidation. (Reaction conditions: temperature = 403 K, [phenol] = 1 wt%).

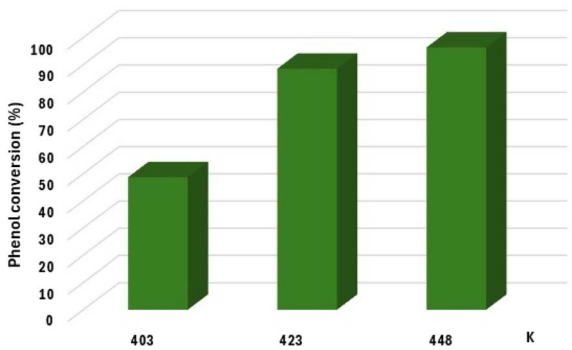

Fig. 7 Influence of temperature on phenol oxidation. (Reaction conditions: pressure = 0.6 MPa, [phenol] = 1 wt%).

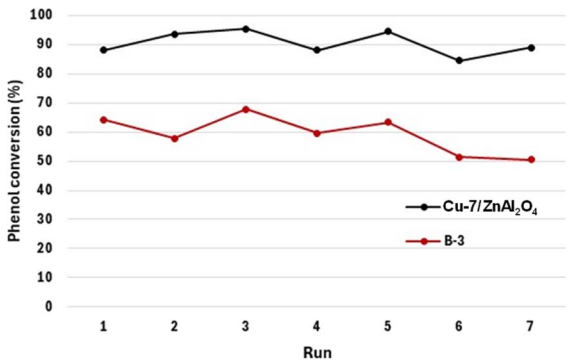

Fig. 9 Reusability of catalysts in phenol oxidation. (Reaction conditions: temperature = 403 K, pressure = 0.6 MPa, [phenol] = 1 wt%).

Table 7 CWAO performance of various catalysts for phenol conversion

Catalyst	Reaction conditions[a]	Maximum conversion (%)	Reaction time[b] (h)	Reactor type	Stability (%)	Reference
CuO–ZnO/γ-Al_2O_3	413 K, 4.7 MPa [phenol = 0.5]	80	192	Tubular	50	35
10% CuO/γ-Al_2O_3	413 K, 0.9 MPa [phenol = 0.5]	85	800	Tubular	47	49
Cu-Fe/$ZnAl_2O_4$	423 K, 1.0 MPa [phenol = 0.15]	95	32	Autoclave	99	32
Pt/Graphite	423 K, 1.8 MPa [phenol = 0.18]	95	4	Continuous stirred tank	100	52
MnCeOx	343 K, 2.0 MPa [phenol] = 0.1	90	900	Autoclave	100	14
Cu-Zn/$FeAl_2O_4$	443 K, 1.0 MPa [phenol] = 0.43	100	40	Autoclave	100	62
Cu-Ce/AC	433 K, 3.0 MPa [phenol] = 0.1	99	49	Fixed bed	98	63
CuO/$ZnAl_2O_4$	403 K, 0.6 MPa [phenol] = 1.0	95	54	Semi-batch	100	This work

[a] Phenol concentration in wt%. [b] In experiments with catalyst recycling, the reaction time was calculated as the number of cycles times the reaction time of each cycle.

Several studies have reported on the stability of catalysts for phenol oxidation with good stability over time. Most of them have utilized lower phenol concentration and higher temperature and pressure, conditions under which phenol is easier to be converted (Table 7).

4.5 Phenol oxidation employing a refinery stream

These evaluations were conducted on a spent soda sample from the primary gasoline sweetening unit at the Salamanca Refinery in Guanajuato, México; the reaction conditions were those reported in Table 3. The characterization of this sample is shown in Table 8.

From Fig. 10, it is noteworthy to state that the phenol conversions in caustic soda were higher than in synthetic solutions. This can be explained by the fact that phenol in caustic soda is transformed into sodium phenolate, which is more than three times more soluble than phenol and its reactivity has been reported to be greater than that of phenol;[58,64] in addition, the refinery stream had lower phenol concentration than that of the synthetic solution and was easier to remove; a slight and constant decrease in phenol oxidation was observed with the Cu-7/$ZnAl_2O_4$ catalyst.

Table 8 Characterization of refinery spent soda

Parameter	Value
Specific gravity	1.16
Soda, wt%	3.78
Phenol, wt%	0.17
Sodium mercaptans, ppm	138
Sulfides, ppm	2148
Free soda, wt%	4.37
pH	13.5

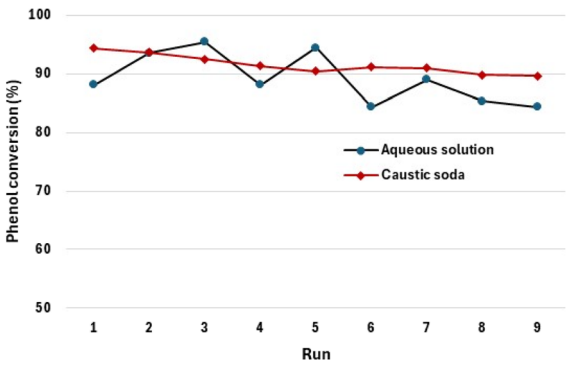

Fig. 10 Oxidation of phenol with refinery spent soda. (Reaction conditions: temperature = 403 K, pressure = 0.6 MPa, [phenol] = 0.17 wt%).

The metal content was quantified after each reaction run by atomic absorption in the caustic solution to determine the metal leaching of the Cu-7/$ZnAl_2O_4$ catalyst. The average analysis showed < 5 ppm of Al, 5 ppm of Cu, and 1 ppm of Zn. The amount of leached metals was lower than in synthetic phenol solutions, which could be the reason why the deactivation of the catalysts was not so severe, keeping the phenol conversion almost constant.

Metal lixiviation at high pH is not widely reported in active catalysts; most of the literature addresses this topic from pH 7 downwards. Alkaline and acid leaching is used to recover metals in coal and fly ash; most metals are easily removed by acid treatment, while alkali leaching is performed due to the high affinity of the leachant hydroxyl ion to form soluble sodium hydrated silicate and aluminate and sodium aluminosilicate compounds, nevertheless, the demineralization degree decreases at higher NaOH concentration because some metals have low solubility in alkalis such as Zn and Cu.[65,66] The recovery of metals from selective catalytic reduction (SCR), hydrotreating, and sulfuric acid spent catalysts is performed under acid or alkali conditions; vanadium, chromium, zinc, and copper can be easily recovered in acid medium, but Ni is not dissolved by sodium hydroxide, while Mo is leached only at 433 K in a caustic autoclaving process.[67–69]

It has been reported that there is less copper leaching at alkaline pH in the phenol oxidation reaction, as well as less deactivation and therefore, longer catalyst life.[16,36,70] In this work, copper, zinc, and aluminum resisted the action of the alkaline solution of the caustic sample from a refining process with very low metal leaching in the phenol oxidation process with CWAO, because the produced organic acids were neutralized with NaOH, making this process suitable for the treatment of these spent soda streams.

5 Conclusions

Bulk, alumina-supported, and aluminate-supported Cu–Al and Zn–Al catalysts were successfully synthesized and evaluated for

phenol oxidation by CWAO. The results demonstrate that catalyst structure and metal–support interactions play a decisive role in both activity and stability. Bulk catalysts showed activity strongly dependent on textural properties, while γ-Al_2O_3-supported catalysts exhibited enhanced phenol conversion due to improved metal dispersion and accessibility of active sites.

Among the studied materials, CuO supported on zinc aluminate spinels displayed the best overall performance, combining high phenol conversion with excellent stability and low metal leaching. Notably, these catalysts maintained their activity during multiple runs using real caustic refinery effluents, where the alkaline environment neutralized organic acids formed during oxidation, effectively suppressing metal dissolution.

This work provides the first systematic demonstration of stable CWAO operation for phenol removal in caustic refinery streams, highlighting the potential of Cu–Al and Zn–Al catalysts, particularly aluminate spinels, as viable materials for industrial wastewater treatment. The insights obtained here contribute to the rational design of robust catalysts for the processing of highly alkaline industrial effluents.

Pressure and temperature are operating conditions that determine the solubility of oxygen in aqueous solutions. Studies on these variables have shown that operating at temperatures up to 448 K favored the phenol oxidation reaction; temperatures and pressures above 1.5 MPa have little influence on phenol conversion. Conditions above these values should be avoided to prevent increasing operating costs.

Author contributions

Jorge F. Palomeque-Santiago conceptualization, investigation, methodology. José J. Castro-Arellano supervision, writing – review.

Conflicts of interest

There are no conflicts to declare.

Data availability

The data supporting this article is confidential to the Mexican Petroleum Institute and is only available through the corresponding author upon reasonable request.

Acknowledgements

This work was funded by the Mexican Petroleum Institute under Project E0C-7335. The authors thank Chemist Erika Díaz Aranda for the fruitful discussions during the completion of this work.

References

1 N. V. Pradeep, S. Anupama, K. Navya, H. N. Shalini, M. Idris and U. S. Hampannavar, *Appl. Water Sci.*, 2015, **5**, 105–112.
2 T. Al-Khalid and M. H. El-Naas, *Crit. Rev. Environ. Sci. Technol.*, 2012, **42**, 1631–1690.
3 W. F. Elmobarak, B. H. Hameed, F. Almomani and A. Z. Abdullah, *Catalysts*, 2021, **11**, 782.
4 Y. Zhou, F. Gao, Y. Zhao and J. Lu, *J. Saudi Chem. Soc.*, 2014, **18**, 589–592.
5 A. Quintanilla, J. A. Casas and J. J. Rodriguez, *Appl. Catal., B*, 2010, **93**, 339–345.
6 I. Benhamed, L. Barthe, R. Kessas, H. Delmas and C. Julcour, *Environ. Technol.*, 2018, **39**, 2761–2770.
7 S. K. Bhargava, J. Tardio, J. Prasad, K. Föger, D. B. Akolekar and S. C. Grocott, *Ind. Eng. Chem. Res.*, 2006, **45**, 1221–1258.
8 A. Sadana, *J. Catal.*, 1974, **35**, 140–152.
9 S. Hamoudi, A. Sayari, K. Belkacemi, L. Bonneviot and F. Larachi, *Catal. Today*, 2000, **62**, 379–388.
10 M. A. L. Rocha, G. Del Ángel, G. Torres-Torres, A. Cervantes, A. Vázquez, A. Arrieta and J. N. Beltramini, *Catal. Today*, 2015, **250**, 145–154.
11 H. Chen, A. Sayari, A. Adnot and F. Larachi, *Appl. Catal., B*, 2001, **32**, 195–204.
12 B. T. Dossumova, L. R. Sassykova, T. V. Shakiyeva, D. Muktaly, A. A. Batyrbayeva and M. A. Kozhaisakova, *ChemEngineering*, 2024, **8**, 8.
13 S.-K. Kim and S.-K. Ihm, *Top. Catal.*, 2005, **33**, 171–179.
14 L. Geng, B. Chen, J. Yang, C. Shui, S. Ye, J. Fu, N. Zhang, J. Xie and B. Chen, *Appl. Catal., A*, 2020, **604**, 117774.
15 A. Fortuny, J. Font and A. Fabregat, *Appl. Catal., B*, 1998, **19**, 165–173.
16 P. M. Álvarez, D. McLurgh and P. Plucinski, *Ind. Eng. Chem. Res.*, 2002, **41**, 2153–2158.
17 A. Sadana and J. R. Katzer, *Ind. Eng. Chem. Fundam.*, 1974, **13**, 127–134.
18 J. Levec, *Appl. Catal.*, 1990, **63**, L1–L5.
19 A. Pintar and J. Levec, *J. Catal.*, 1992, **135**, 345–357.
20 A. Alejandre, F. Medina, A. Fortuny, P. Salagre and J. E. Sueiras, *Appl. Catal., B*, 1998, **16**, 53–67.
21 C. Lai, T. He, X. Li, F. Chen, L. Yue and Z. Hou, *Appl. Clay Sci.*, 2019, **181**, 105253.
22 J. F. Akyurtlu, A. Akyurtlu and S. Kovenklioglu, *Catal. Today*, 1998, **40**, 343–352.
23 A. Devard, P. Brussino, F. A. Marchesini and M. A. Ulla, *J. Environ. Chem. Eng.*, 2019, **7**, 103201.
24 S.-K. Kim, K.-H. Kim and S.-K. Ihm, *Chemosphere*, 2007, **68**, 287–292.
25 N. A. Sacco, M. E. Lovato, F. A. Marchesini and A. V. Devard, *J. Hazard. Mater. Lett.*, 2022, **3**, 100059.
26 S. A. Hosseini, K. Farhadi, S. Siahkamari and B. Azizi, *Can. J. Chem.*, 2017, **95**, 87–94.
27 C. G. Anchieta, D. Sallet, E. L. Foletto, S. S. Da Silva, O. Chiavone-Filho and C. A. O. Do Nascimento, *Ceram. Int.*, 2014, **40**, 4173–4178.
28 A. S. Diez, S. Schlichter, V. Tomanech, E. V. P. Miner, M. Alvarez and M. Dennehy, *J. Environ. Chem. Eng.*, 2017, **5**, 3690–3697.
29 E. Saputra, S. Muhammad, H. Sun, H.-M. Ang, M. O. Tadé and S. Wang, *J. Colloid Interface Sci.*, 2013, **407**, 467–473.

30 A. Xu, M. Yang, R. Qiao, H. Du and C. Sun, *J. Hazard. Mater.*, 2007, **147**, 449–456.
31 C. Moreno-Castilla, M. V. López-Ramón, M. Á. Fontecha-Cámara, M. A. Álvarez and L. Mateus, *Nanomaterials*, 2019, **9**, 901.
32 A. Xu, M. Yang, H. Du and C. Sun, *Catal. Commun.*, 2006, **7**, 513–517.
33 A. Santos, P. Yustos, A. Quintanilla and F. García-Ochoa, *Top. Catal.*, 2005, **33**, 181–192.
34 A. Santos, E. Barroso and F. García-Ochoa, *Catal. Today*, 1999, **48**, 109–117.
35 A. Fortuny, *J. Hazard. Mater.*, 1999, **64**, 181–193.
36 R. R. Zapico, P. Marín, F. V. Díez and S. Ordóñez, *J. Environ. Chem. Eng.*, 2017, **5**, 2570–2578.
37 A. Coelho, A. V. Castro, M. Dezotti and G. L. Sant'Anna, *J. Hazard. Mater.*, 2006, **137**, 178–184.
38 G. Busca, S. Berardinelli, C. Resini and L. Arrighi, *J. Hazard. Mater.*, 2008, **160**, 265–288.
39 D. Ma, H. Yi, C. Lai, X. Liu, X. Huo, Z. An, L. Li, Y. Fu, B. Li, M. Zhang, L. Qin, S. Liu and L. Yang, *Chemosphere*, 2021, **275**, 130104.
40 O. Abdelwahab, N. K. Amin and E.-S. Z. El-Ashtoukhy, *J. Hazard. Mater.*, 2009, **163**, 711–716.
41 M. S. Hellal, K. H. Kamal and E. M. Abou-Taleb, *Discov. Sustain.*, 2025, **6**, 833.
42 W. Al Hashemi, M. A. Maraqa, M. V. Rao and M. M. Hossain, *Desalin. Water Treat.*, 2015, **54**, 660–671.
43 S.-H. Sheu and H.-S. Weng, *Water Res.*, 2001, **35**, 2017–2021.
44 R. Alnaizy, *Environ. Prog.*, 2008, **27**, 295–301.
45 B. Y. Jibril, A. Y. Atta, Y. M. Al-Waheibi and T. K. Al-Waheibi, *J. Ind. Eng. Chem.*, 2013, **19**, 1800–1804.
46 A. Sadana, *Ind. Eng. Chem. Process Des. Dev.*, 1980, **19**, 324–325.
47 A. Sadana, *Ind. Eng. Chem. Process Des. Dev.*, 1979, **18**, 50–56.
48 A. Santos, P. Yustos, A. Quintanilla, S. Rodríguez and F. García-Ochoa, *Appl. Catal., B*, 2002, **39**, 97–113.
49 A. Alejandre, F. Medina, P. Salagre, A. Fabregat and J. E. Sueiras, *Appl. Catal., B*, 1998, **18**, 307–315.
50 M. K. Zamisa, T. W. Seadira and S. J. Baloyi, *Environ. Pollut.*, 2024, **361**, 124842.
51 G. Lafaye, J. Barbier and D. Duprez, *Catal. Today*, 2015, **253**, 89–98.
52 Z. P. G. Masende, B. F. M. Kuster, K. J. Ptasinski, F. J. J. G. Janssen, J. H. Y. Katima and J. C. Schouten, *Catal. Today*, 2003, **79–80**, 357–370.
53 J. Levec and A. Pintar, *Catal. Today*, 1995, **24**, 51–58.
54 L. Zhou, H. Cao, C. Descorme and Y. Xie, *Front. Environ. Sci. Eng.*, 2018, **12**(1), 1–20.
55 J. A. Zazo, J. A. Casas, A. F. Mohedano, M. A. Gilarranz and J. J. Rodríguez, *Environ. Sci. Technol.*, 2005, **39**, 9295–9302.
56 M. K. Sushma and A. K. Saroha, *J. Environ. Manage.*, 2018, **228**, 169–188.
57 M. Martín-Hernández, J. Carrera, M. E. Suárez-Ojeda, M. Besson and C. Descorme, *Appl. Catal., B*, 2012, **123–124**, 141–150.
58 F. J. Rivas, S. T. Kolaczkowski, F. J. Beltrán and D. B. McLurgh, *Chem. Eng. Sci.*, 1998, **53**, 2575–2586.
59 K. Miserli, D. Kogola, I. Paraschoudi and I. Konstantinou, *Chem. Eng. J. Adv.*, 2022, **9**, 100201.
60 Sushma and A. K. Saroha, *J. Environ. Chem. Eng.*, 2019, **7**, 103382.
61 A. Quintanilla, J. L. Diaz De Tuesta, C. Figueruelo, M. Munoz and J. A. Casas, *Catalysts*, 2019, **9**, 516.
62 A. Xu and C. Sun, *Environ. Technol.*, 2012, **33**, 1339–1344.
63 G. Li, S. Chai, G. Zhang, J. Liu, Y. Zhang, Y. Lv, Y. Wang and Y. Zhao, *J. Environ. Chem. Eng.*, 2022, **10**, 108228.
64 L. V. Shibaeva, *Kinet. Catal.*, 1969, **10**, 832–836.
65 Y. Zhang, X. Feng, L. Qian, J. Luan and B. Jin, *J. Environ. Chem. Eng.*, 2021, **9**, 105997.
66 S. Behera, U. Kumari and B. Meikap, *J. Min. Metall., Sect. A*, 2018, **54**, 1–24.
67 Z. Dai, L. Wang, H. Tang, Z. Sun, W. Liu, Y. Sun, S. Su, S. Hu, Y. Wang, K. Xu, L. Liu, P. Ling and J. Xiang, *Chemosphere*, 2018, **207**, 440–448.
68 A. Ognyanova, A. T. Ozturk, I. De Michelis, F. Ferella, G. Taglieri, A. Akcil and F. Vegliò, *Hydrometallurgy*, 2009, **100**, 20–28.
69 S. Huang, Z. Zhao, X. Chen and F. Li, *Int. J. Refract. Met. Hard Mater.*, 2014, **46**, 109–116.
70 A. Santos, P. Yustos, A. Quintanilla and F. Garcia-Ochoa, *Chem. Eng. Sci.*, 2005, **60**, 4866–4878.